PCCP

Physical Chemistry Chemical Physics

www.rsc.org/pccp

Volume 13 | Number 40 | 28 October 2011 | Pages 17901–18232

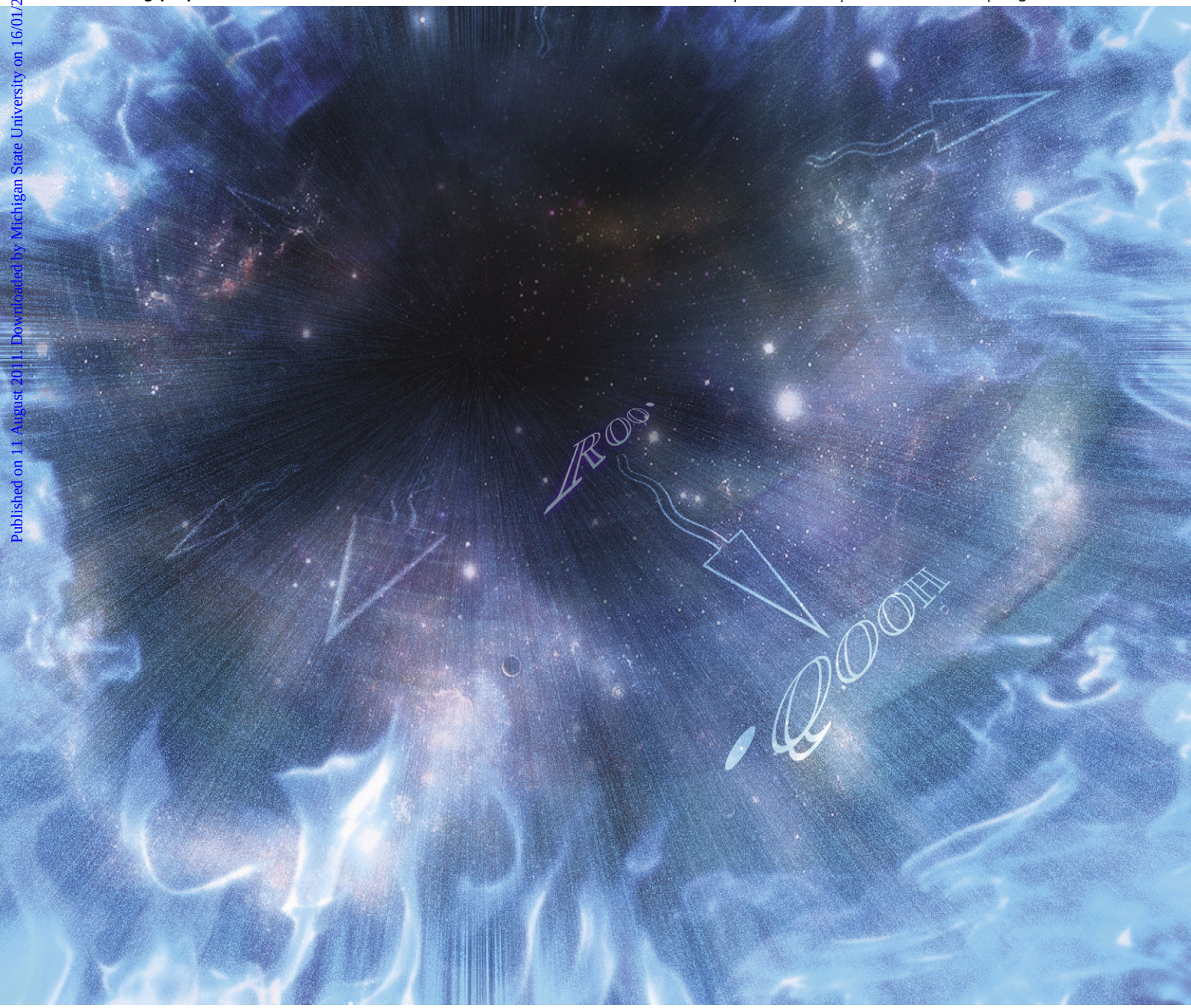

ISSN 1463-9076

COVER ARTICLE
Zhang and Dibble
Impact of tunneling on hydrogen-migration of the *n*-propylperoxy radical

PERSPECTIVE
Zehnacker *et al.*
The role of weak hydrogen bonds in chiral recognition

1463-9076(2011)13:40;1-U

PCCP

View Article Online
Dynamic Article Links

Cite this: *Phys. Chem. Chem. Phys.*, 2011, **13**, 17969–17977

www.rsc.org/pccp

PAPER

Impact of tunneling on hydrogen-migration of the *n*-propylperoxy radical†

Feng Zhang and Theodore S. Dibble*

Received 25th May 2011, Accepted 11th July 2011
DOI: 10.1039/c1cp21691k

The kinetics of three unimolecular reactions of the *n*-propylperoxy radical were studied by canonical variational transition state theory and multidimensional small curvature tunneling (SCT). The reactions studied were 1,5 and 1,4 H-migration, and HO_2 elimination. Benchmark calculations were carried out at the CCSD(T) level in order to determine which density functional to use for SCT calculations for each reaction. For 1,5 and 1,4 H-migration, and HO_2 elimination, the M05-2X, B3LYP and B1B95 functionals, respectively, performed closest to the benchmark when coupled to the 6-311 + G(2df,2p) basis set. The SCT tunneling corrections, $\kappa(T)$, computed here were much larger than those calculated from the Wigner or zero-curvature tunneling treatments at low temperatures, but the asymmetric Eckart method works surprisingly well in these three reactions. Comparison of energy-dependent transmission coefficients, $\Gamma(E)$, indicates that not only the magnitude, but also the sign, of the error in the Eckart approximation is a function of energy; therefore, the error introduced by using the Eckart approach depends strongly on the steady state energy distribution. These results may provide guidance for future studies of tunneling effects in reactions of other peroxy radicals.

1. Introduction

Alkyl peroxy radicals ($ROO^{\bullet}$) are critical intermediates in atmospheric and combustion chemistry. Intramolecular H-migration reaction channels of alkyl peroxy radicals can lead to radical chain branching, which is necessary for autoignition of diesel fuel.[1] A concerted HO_2 elimination channel competes with H-migration channels and tends to delay autoignition. These unimolecular reactions of alkyl peroxy radicals (illustrated in Scheme 1 for the *n*-propylperoxy radical) and subsequent reactions are responsible for the negative temperature coefficient (NTC) behavior of ignition delay times of large alkanes at around 500–800 K.[1–5] Because of its importance in low-temperature combustion, peroxy radical chemistry has been studied extensively both in experiments and kinetic modeling.[1–7] The organic radical product of H-migration of peroxy radicals, commonly labelled QOOH, has never been detected by any experimental method, let alone in a manner that would allow for kinetic studies. This means that theoretical studies play a vital role in understanding this chemistry.[2,3,8–10] This chemistry is also important for ignition delay in homogeneous charge compression ignition engines, an engine type being developed with the goal of combining the high power of diesel engines with the low emissions of gasoline engines.[11,12]

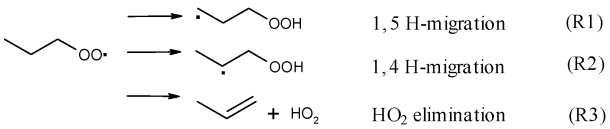

Scheme 1

At the 500–800 K temperatures relevant to autoignition, tunneling may significantly influence reaction rate constants for the H-migration reactions. Therefore, we were surprised to notice that previous theoretical studies of alkyl peroxy radical chemistry had only employed approximate one-dimensional tunneling treatments,[8,13–19] such as the Wigner[20] or Eckart[21] models. The Wigner and Eckart methods treat tunneling along one-dimensional potential curves, do not use the correct shape of the barrier, and assume constant reduced mass along the reaction path; however, reliable treatments of tunneling should include the full multi-dimensional nature of the potential surface.[22–27] Unimolecular reactions of alkyl peroxy radicals in combustion usually occur in the fall-off region rather than at the high-pressure limit, and tunneling can cause enormous changes in rate constants for H-migration reactions in the fall-off region.[28,29] Therefore, before one chooses a one-dimensional tunneling model to be used in computing pressure

Department of Chemistry, College of Environmental Science and Forestry, State University of New York, Syracuse, NY, USA 13210. E-mail: tsdibble@esf.edu

† Electronic supplementary information (ESI) available: Cartesian coordinates (in Å) of all stationary points for R1 thru R3 at the M05-2X/MG3S level; barrier heights and reaction energies for R1 thru R3; multidimensional tunneling corrections of R1 based on the reaction path of $-0.5 \sim 0.5$ Å; tunneling corrections computed by different approximations for R1 and R2; transmission coefficients computed by different approximations for R1 and R2; high pressure limit rate constants by CVT/SCT for R1 to R3. See DOI: 10.1039/c1cp21691k

dependent rate constants, it is valuable to check its reliability against a multidimensional tunneling treatment.

In this work, the impact of tunneling on unimolecular reactions of the *n*-propyl peroxy radical (1-$C_3H_7OO^\bullet$)[3,8,13,14,30–33] is investigated with multi-dimensional tunneling treatments as the first step in investigating tunneling in alkyl peroxy radical reactions, generally. Scheme 1 shows the three reactions addressed in this work. Rate constants are calculated by so-called "direct dynamics" calculations using canonical variational transition state theory (CVT)[22,24] with small curvature tunneling (SCT) calculations. The CVT/SCT calculations require determination, not only of the energy along the minimum energy path (MEP), but also gradients and Hessians at numerous points along the MEP. This means that very efficient electronic structure methods are required, so density functional theory (DFT) methods were used. Different functionals were selected for each of the three reactions based on comparison of DFT activation barriers and reaction energies to results of benchmark calculations. This work aims to provide a reference for choosing tunneling treatments in future studies of larger alkyl peroxy radicals, so tunneling corrections were also computed by one-dimensional approximations (Wigner and Eckart) and zero-curvature tunneling (ZCT) for comparison with the SCT results.

2. Methodology

2.1 *Ab initio* and DFT calculations

Ab initio and DFT calculations were performed using the GAUSSIAN09 program.[34] The nature of stationary points was checked by vibrational analysis. All the DFT calculations were performed using "ultrafine" integration grids, which request a pruned (99, 590) grid-99 radial shell and 590 angular points per shell. The default grid in GAUSSIAN09 is the pruned (75, 302) grid. The importance of using an ultrafine grid for thermochemistry and kinetics has been demonstrated by Simón and Goodman.[35] Spin-unrestricted wavefunctions were used in all calculations on radicals. All conformers of reactants and products were optimized with the M05-2X functional[36,37] together with the 6-311+G(2df,2p) basis set (hereafter MG3S), to determine the lowest energy conformer.

The first task was to get reliable relative energies to help evaluate which combinations of basis set and functional to use for direct dynamics calculations. To this end, single point energies were computed by using coupled cluster theory with single and double excitations and a quasi-perturbative treatment of connected triple excitations (CCSD(T))[38] on the saddle points and the lowest energy conformers of reactants and products determined previously. CCSD(T) calculations used correlation-consistent polarized triple-zeta basis set with minimal augmented diffuse functions: maug-cc-pVTZ.[39]

We then tested several combinations of functionals and basis sets, including M05-2X,[36,37] M06-2X,[40] B3LYP,[41,42] BMK,[43] B3PW91,[44] MPW3PPBE,[45] ωB97X,[46] B1B95,[47] B98,[48] and CAM-B3LYP[49] with the MG3S basis set, and, in selected cases, with the 6-31+G(d,p), 6-31+G(2df,2p), 6-311+G(2d,2p), and 6-311+G(d,p) basis sets. The DFT method/basis set combination which gave the minimum mean unsigned error (MUE) of barrier height and reaction energy for each reaction was chosen for direct dynamics calculations on that reaction. A different functional was selected for each of the three reactions.

2.2 Direct dynamics

Variational transition state theory (VTST) minimizes the recrossing of the barrier by variationally locating an alternative transition-state dividing surface orthogonal to the MEP, instead of relying on the saddle point defined by conventional TST.[24] In a canonical ensemble, the VTST rate constant is given by

$$k^{\mathrm{CVT}}(T) = \min_{s} k^{\mathrm{TST}}(T,s) = \sigma \frac{1}{\beta h} \frac{Q^{\neq}(T, s_*^{\mathrm{CVT}})}{Q^{\mathrm{R}}(T)} \exp[-\beta V_{\mathrm{MEP}}(s_*^{\mathrm{CVT}})] \qquad (1)$$

where s is the reaction coordinate, $s = 0$ at the saddle point; s_*^{CVT} is the value of s at which $k^{\mathrm{TST}}(T, s)$ has a minimum; σ is the reaction-path symmetry number, which is unity for the three reactions studied in this work;[50] $Q^{\neq}(T, s_*^{\mathrm{CVT}})$ and $Q^{\mathrm{R}}(T)$ are the partition functions (rotational, vibrational, and electronic) of the transition state and reactant, respectively.

Direct dynamics calculations were performed using the POLYRATE[51] and GAUSSRATE[52] programs; the latter is the interface between POLYRATE and GAUSSIAN. The MEP was first optimized within a small range of the reaction path: -0.5 Å $< s <$ 0.5 Å (where distances are scaled to a reduced mass of 1 amu) by using the Page–McIver integrator[53] with a step size of 0.0025 Å.

The Hessian was computed every 9 steps. Based on this small range MEP, the reaction path was extended to -3 Å $< s <$ 3 Å by the algorithm of interpolated variational transition-state theory by mapping (IVTST-M).[54] The full direct dynamics is denoted by IVTST-M-44/402, meaning that straight direct dynamics provided energies and gradients at 402 points (including 3 stationary points) and Hessians at 44 points. In our direct dynamics calculations, redundant curvilinear internal coordinates[55] and the harmonic-oscillator (HO) approximation were employed for generalized normal mode analyses. The frequency scaling factor used in all calculations is chosen as 0.975 for M05-2X, 0.998 for B3LYP and 0.987 for B1B95 with the MG3S basis set.[56] The effect of hindered rotors on rate constants was included as detailed below.

To test that the step size of 0.0025 Å was small enough, test calculations were carried out for the 1,5 H-migration in the range -0.5 Å $< s <$ 0.5 Å with a step size of 0.0015 Å and 0.0025 Å with M05-2X and the small 6-31+G(d,p) basis set. The CVT rate constant was converged to better than 1% at all temperatures. The tunneling corrections, $\kappa(T)$, specified in eqn (2), below, depend on the step size more than does the variational rate constants. Based on the extended long range reaction path by the IVTST-M method, SCT and ZCT corrections were converged to within 10% and 15%, respectively, at 300 K, and better than 10% at higher temperatures. We assume that similar convergence holds at the MG3S basis set used in the results reported below.

2.3 Tunneling and hindered rotor treatments

To correct for tunneling, the classical rate constant in eqn (1) is multiplied by a temperature-dependent tunneling correction, $\kappa(T)$:

$$k_{QM}^{CVT}(T) = \kappa(T)k^{CVT}(T) \quad (2)$$

Assuming a parabolic potential near the saddle point, $\kappa(T)$ can be computed by first order perturbation theory; this is the approach of Wigner. Wigner's tunneling formula only has one variable—the imaginary frequency $\upsilon^{\neq}$. If the quantum tunneling effect is a small deviation from classical behavior, corresponding to high temperature or small $\upsilon^{\neq}$, the tunneling correction factor can be truncated at the first term when solving the Schrödinger equation by perturbation theory, leading to eqn (3).

$$\kappa_{Wigner}(T) = 1 + \frac{1}{24}\left(\frac{h\upsilon^{\neq}}{k_B T}\right)^2 \quad (3)$$

As an advance over the parabolic potential used in Wigner approximation, Eckart evaluated an analytic potential function fitted by the energies of three stationary points and the imaginary frequency, given as:[21]

$$V_{Eckart}(s) = \frac{Ae^{2\pi s/L}}{1+e^{2\pi s/L}} + \frac{Be^{2\pi s/L}}{(1+e^{2\pi s/L})^2} \quad (4)$$

where s is the reaction coordinate, and A, B, and L are parameters calculated from forward and reverse barrier heights and the imaginary frequency. The transmission coefficient is computed by solving the Schrödinger equation to obtain:[21,57]

$$\Gamma_{Eckart}(E) = \frac{\cos h(a+b) - \cos h(a-b)}{\cos h(a+b) + \cos h(d)} \quad (5)$$

Equations for parameters a, b, and d in eqn (5) can be found in the literature.[21,57] A reduced mass is required when using eqn (5), which is chosen as 1 amu. Convoluting $\Gamma_{Eckart}(E)$ with the Boltzmann distribution gives the temperature dependent tunneling correction factor:

$$\kappa_{Eckart}(T) = \frac{\exp(E_0/k_B T)}{k_B T}\int_0^{\infty} \Gamma_{Eckart}(E)\exp(-E/k_B T)dE \quad (6)$$

The Wigner and asymmetric Eckart tunneling corrections are often used because of their simplicity, despite that they can introduce large errors. In contrast to the one-dimensional tunneling treatments, multi-dimensional tunneling corrections require energies, gradients and Hessians along the reaction path. The adiabatic ground state potential energy (V_a^G) is computed from the sum of the potential, V_{MEP}, along the optimized reaction path and the zero-point vibrational energy ε_{int}^G of modes orthogonal to the reaction coordinate, *i.e.*

$$V_a^G(s) = V_{MEP}(s) + \varepsilon_{int}^G(s) \quad (7)$$

Multidimensional tunneling treatments address two key issues: (1) the contribution of vibrational energies from all vibrational modes, which changes the shape of the effective potential for tunneling; (2) the coupling between the reaction coordinate and orthogonal vibrational modes, known as the corner-cutting effect, which manifests itself by the curvature of the reaction path. This shortens the tunneling path and increases the tunneling.[22] The first aspect was included by Skodje and Truhlar in the zero-curvature tunneling approximation.[22–24] Because of its neglect of the corner-cutting effect, ZCT seriously underestimates tunneling corrections to rate constants.[24,25] The small- and large-curvature tunneling (SCT and LCT) approximations[22,24] take into account both issues (1) and (2) with respect to small and large curvature, respectively. Both ZCT and SCT use the semiclassical WKB approximation. The semiclassical transmission probability as a function of E is given by:[22,57]

$$\Gamma_{SCT}(E) = \begin{cases} 0 & E < E_0 \\ [1+e^{2\theta(E)}]^{-1} & E_0 \le E \le V_a^G \\ 1 - \Gamma_{SCT}(2V_a^G - E) & V_a^G \le E \le 2V_a^G - E_0 \\ 1 & 2V_a^G - E_0 < E \end{cases} \quad (8)$$

where E_0 is the quantum threshold energy for tunneling (corresponding to V_a^G at $s = +\infty$ for these endothermic reactions), $\theta(E)$ is the imaginary action integral along the reaction path V_a^G.

$$\theta(E) = \hbar^{-1}\int_{s<}^{s>} ds\{2\mu_{eff}[V_a^G(s) - E]\}^{1/2} \quad (9)$$

where $s<$ and $s>$ are the classical turning points (where V_a^G equals E), μ_{eff} is the effective mass of the tunneling motion along the reaction coordinate, which is a function of the curvature (*i.e.* coupling between the reaction coordinate and the transverse modes) at a given value of s. The explicit calculation of μ_{eff} is complicated and can be found elsewhere.[22,58] Within the ZCT approximation, μ_{eff} is assumed as a constant, neglecting the corner-cutting effect. Therefore, ZCT can be considered as a rough approximation of SCT. Temperature dependent tunneling corrections, $k_{SCT}(T)$, are obtained as in eqn (6).

A LCT calculation is necessary when the MEP is highly curved, which is usually not the case for unimolecular reactions.[59,60] Where there may be a mix of small and large curvature, a better choice is to use microcanonically optimized multidimensional tunneling (μOMT), which calculates the microcanonical transmission probability, $\Gamma(E)$, as the larger of the microcanonical SCT and LCT values.[61] Unfortunately, LCT calculations require much more computational time than SCT, and cannot be used with the IVTST-M algorithm. In this work, we only performed μOMT calculations based on the reaction path from −0.5 Å to 0.5 Å with the small 6-31+G(d,p) basis set for the two H-migration reactions to check the importance of LCT tunneling in these systems. Conventional TST and CVT with Wigner and multidimensional tunneling corrections were carried out with programs POLYRATE and GAUSSRATE. Eckart tunneling was computed by a RRKM subroutine in the UNIMOL program suite.[62]

As seen from eqn (1), accurate CVT rate constants require proper treatment of partition functions for transition states and reactants. Internal rotations are very anharmonic, so treating them as harmonic vibrations may lead to large errors in rate constants. In this work, the hindered rotor partition function for each torsional mode is obtained by the torsional eigenvalue summation (TES) method,[63,64] which requires

solving the Schrödinger equation for the hindrance potential of the rotor. The hindrance potential is computed by a relaxed scan with 10° resolution at the same theoretical level as in the direct dynamics calculations. The potential is fitted by a Fourier series up to 18 terms to numerically solve the Schrödinger equation. Fitting and solving the Schrödinger equation was carried out using the program T-Chem.[64,65] Rate constants computed in POLYRATE, *i.e.* k_{QM}^{CVT} in eqn (2), using the HO approximation were corrected for hindered rotor (HR) effects by the following simple equation:

$$k_{QM}^{CVT,HR}(T) = C(T)k_{QM}^{CVT,HO}(T)$$
$$C(T) = \frac{Q_{TS}^{HR}(T)}{Q_{TS}^{HO}(T)}\frac{Q_{R}^{HO}(T)}{Q_{R}^{HR}(T)} \quad (10)$$

where $Q_{TS}^{HR}(T)$ and $Q_{TS}^{HO}(T)$ are partition functions for the saddle point computed by hindered rotor and harmonic oscillator approximations, respectively; $Q_{R}^{HR}(T)$ and $Q_{R}^{HO}(T)$ are those of the reactant.

3. Results and discussion

3.1 *Ab initio* calculations

Table 1 lists the calculated barrier heights, reaction energies and mean unsigned error (MUE) by our benchmark method and by selected DFT calculations. The complete results of all DFT and basis set tests mentioned in Section 2.1 are shown in the ESI.† On the basis of their agreement with the CCSD(T)/maug-cc-pVTZ results, the M05-2X, B3LYP and B1B95 methods with the MG3S basis set (shown in bold in Table 1) are selected to carry out tunneling calculations for R1, R2 and R3, respectively. The MUEs for barrier heights and reaction energies for these functionals were less than 1.0 kcal mol^{-1}.

Fig. 1 displays the MEP and V_a^G curves for R1 thru R3 optimized by the selected functional together with MG3S basis set. The zero of energy in Fig. 1 is the energy of the *n*-propylperoxy radical without ZPE. The imaginary frequency of a reaction reflects the width of the MEP and gives some sense of the width of V_a^G. The calculated imaginary frequencies of R1, R2 and R3 are 2172, 1836 and 1027 cm^{-1}, respectively. As a result, R3 (HO_2 elimination) has the widest potential curve. The gap between V_{MEP} and V_a^G is caused by the ε_{int}^G correction, see eqn (7). Clearly, ε_{int}^G corrections change not only barrier heights and reaction energies, but also the shape of the potential.

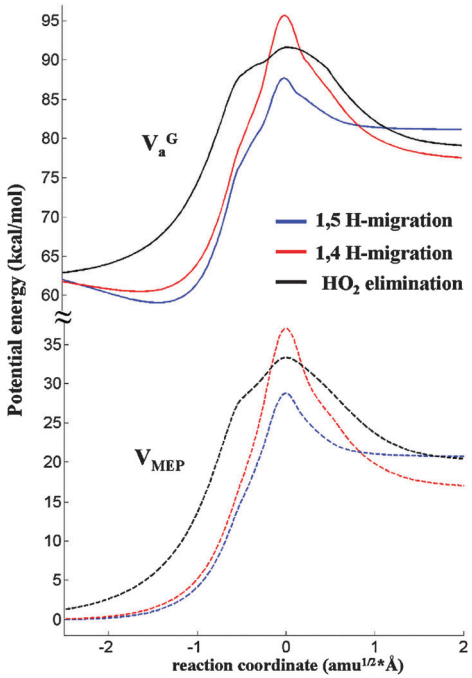

Fig. 1 V_{MEP} and V_a^G for R1, R2 and R3 at M05-2X, B3LYP and B1B95, respectively, with the MG3S basis set.

3.2 Tunneling

Previous work has suggested that LCT is not significant in intramolecular H-migration reactions.[59,60,66] This prediction is validated here by μOMT calculations with a small basis set (6-31+G(d,p)) for the 1,5 and 1,4 H-migration. Table 2 displays tunneling corrections by SCT, LCT and μOMT for 1,4 H-migration, based on the reaction path of −0.5∼0.5 Å. The μOMT correction is exclusively attributable to SCT. Similar results are also obtained for 1,5 H-migration with M05-2X/6-31+G(d,p), as listed in ESI.† This provides some confidence that we can neglect LCT in computing tunneling corrections for R1–R3.

The main purpose of this work is to explore the tunneling effect on unimolecular reactions of the *n*-propylperoxy radical, and to shed light on the extent of the error in the Wigner and Eckart approximations. We start with the 1,4 H-migration, since it has the most significant tunneling effect. Fig. 2(a) displays the tunneling corrections for the 1,4 H-migration computed by four different methods. Tables showing calculated tunneling corrections as a function of temperature and methods are provided in the ESI.†

Table 1 Barrier heights, E_0, and reaction energies, E_{rxn} (in kcal mol^{-1}), including zero point energy (ZPE) correction with frequency scaling

	R1 (1,5 H-migration)			R2 (1,4 H-migration)			R3 (HO_2 elimination)		
Method	E_0	E_{rxn}	MUE	E_0	E_{rxn}	MUE	E_0	E_{rxn}	MUE
CCSD(T)/maug-cc-pVTZ[a]	24.68	16.10	0.00	33.25	13.92	0.00	30.07	16.81	0.00
M052X/MG3S	**25.35**	**17.35**	**0.96**	35.06	14.43	1.16	33.92	19.27	3.16
B3LYP/MG3S	24.47	18.75	1.43	**33.04**	**14.61**	**0.45**	26.91	14.10	2.93
B1B95/MG3S	24.59	20.02	2.01	32.75	16.52	1.56	**29.07**	**16.21**	**0.80**

[a] ZPE correction at M05-2X/MG3S.

Table 2 Multidimensional tunneling corrections of 1,4 H-migration based on the reaction path of −0.5∼0.5 Å at B3LYP/6-31+G(d,p)

T/K	ZCT	SCT	LCT	μOMT
500	4.65	9.01	5.51	9.01
600	2.83	4.14	3.09	4.14
700	2.12	2.72	2.23	2.72
800	1.76	2.10	1.82	2.10
900	1.55	1.78	1.59	1.78
1000	1.42	1.58	1.45	1.58

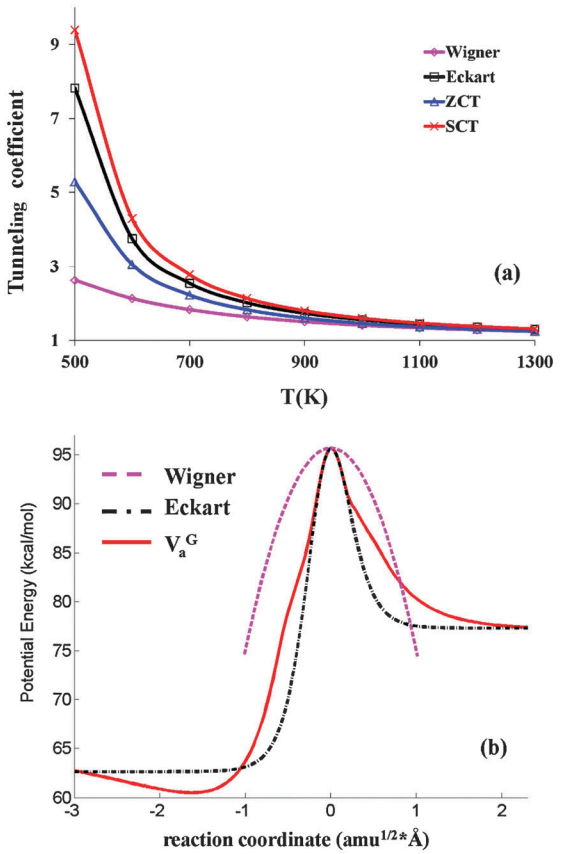

Fig. 2 (a) Tunneling coefficient and (b) potential energy curves of R2 (1,4 H-migration) with different approximations.

At 700 K, a temperature very relevant to diesel autoignition, the Wigner, ZCT, Eckart and SCT tunneling corrections for R2 are 1.8, 2.2, 2.6, and 2.8, respectively, and the discrepancies between methods are much larger at lower temperatures. It is not surprising to find that Wigner's model gives the worst result when compared to the SCT approach, since the Wigner method only accounts for the leading term in the tunneling corrections. Comparison of ZCT and SCT shows that the inclusion of the corner-cutting effect in SCT increases the tunneling correction of 1,4 H-migration over the ZCT value by a factor of 1.2 at 700 K. Fig. 2(b) compares the asymmetric Eckart potential, Wigner parabolic model and the adiabatic ground state potential energy (V_a^G). The energy scale in Fig. 2(b) corresponds to that in Fig. 1, *i.e.*, the electronic energy of the *n*-propylperoxy radical is defined as zero (the Eckart potential in eqn (4) was fit using the three stationary point energies corrected by their ZPE). Apparently, the Eckart potential yields a much narrower potential curve than Wigner, resulting in larger tunneling corrections. It can be seen that the Eckart potential matches V_a^G quite well over much of the reaction coordinate, especially near the top of the barrier.

Tunneling corrections for R1 (1,5 H-migration), shown in Fig. 3, display the same trend as those for 1,4 H-migration. At 700 K, the Wigner, ZCT, Eckart and SCT tunneling corrections are 1.6, 1.6, 1.8, and 2.0, respectively. The Eckart model again works much better than the Wigner and ZCT approximations. Potential energy curves of 1,5 H-migration with the Wigner and Eckart models are shown in the ESI.† The larger imaginary frequency and barrier height for 1,4 H-migration over the 1,5 H-migration lead to more significant tunneling for the former reaction. At 700 K, the tunneling correction for 1,4 H-migration is 1.4 times larger than that of 1,5 H-migration. The tunneling effect on HO_2 elimination is modest due to the heavy atoms involved, and the tunneling corrections computed by all methods are between 1.1 and 1.3 at 700 K.

Fig. 2 and 3 indicate that Eckart's model works much better than Wigner's formula for the two H-migration reactions, and almost as well as the multidimensional SCT model. It might seem reasonable to assume that this holds true for the 1,4 and 1,5 H-migration reactions of many other peroxy radicals, but the agreement relies on a fortuitous cancellation of errors. It is certainly not reasonable to assume that this result holds for other classes of H-migration reactions, as the Eckart model sometimes overestimates the tunneling correction for some reactions.[67–69]

In combustion, peroxy radical chemistry often occurs in the fall-off region rather than at the high pressure limit, and tunneling can be enormously more important in the fall-off region[28,29] because the high-energy tail of the Boltzmann distribution is depleted. It is therefore of interest to compare energy-dependent transmission coefficients, $\Gamma(E)$, computed by various methods, as shown in Fig. 4 for R2. The zero of energy in Fig. 4 is in accord with that in Fig. 1 and Fig. 2(b). Although the $\kappa(T)$ values shown in Fig. 2(a) and 3 indicate significant differences between methods, these differences are dwarfed by the differences in $\Gamma(E)$. As the energy rises to within 8 kcal mol^{-1} of E_0, the Eckart values of $\Gamma(E)$ rise above the SCT values. **A word of caution**: $\Gamma(E)$ values for SCT and ZCT are most reliable for the range of s where V_a^G was

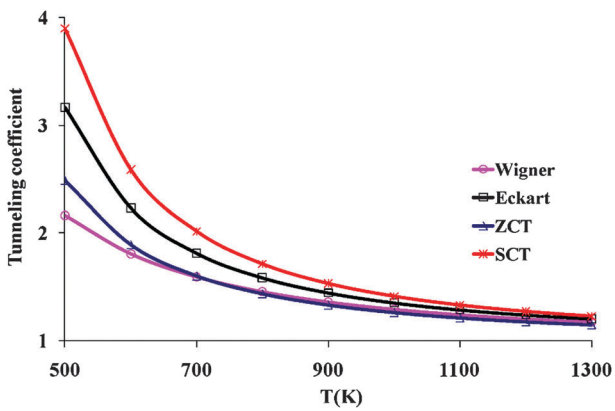

Fig. 3 Tunneling coefficient of 1,5 H-migration with different approximations in the temperature range 500–1300 K.

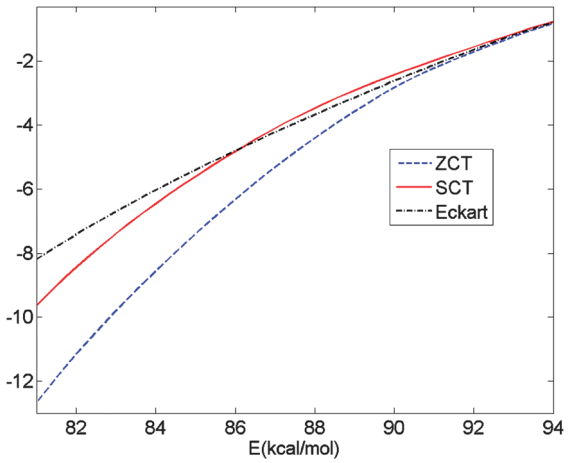

Fig. 4 Transmission coefficients, $\Gamma(E)$, for R2 computed by ZCT, SCT and Eckart approximations.

computed without mapping ($-0.5 < s < 0.5$); therefore, the SCT and ZCT transmission coefficients shown in Fig. 4 are less reliable for $E < 85$ kcal mol^{-1}. At 300 K, the Eckart tunneling correction exceeds the SCT value by a factor of 1.3, whereas at 700 K the SCT value is larger by a factor of 1.2. Clearly, both the extent and sign of the error introduced by using Eckart tunneling will depend in subtle ways on the nature of the energy distribution. The ESI† presents a table of the data in Fig. 4 and an analogous table for R1.

Peroxy radicals also play crucial roles in atmospheric chemistry. Recently, Peeters and coworkers have proposed a new mechanism involving 1,5 and 1,6 H-migration reactions of peroxy radicals formed in the atmospheric oxidation of isoprene at ambient temperatures.[70,71] Isoprene is important because of the enormous quantity emitted to the atmosphere (approximately 500 Mtons year^{-1}) and its presumed role as a scavenger of OH radicals.[72] The mechanism proposed by Peeters and coworkers may help explain the surprisingly large concentrations of OH radicals observed in field studies in the presence of large isoprene emissions.[73] Based on the multi-conformer transition state theory incorporating ZCT tunneling, Peeters *et al.* predicted that the isomerization reactions of isoprene contribute 1–10% of the overall OH generation.[70,74] Our results at temperatures above 500 K have shown that ZCT can seriously underestimate tunneling effects for similar reactions. To give a basis for estimating the error of the ZCT method at atmospherically relevant temperatures, we computed the tunneling effect of 1,5 H-migration for the *n*-propylperoxy radical for $200 \leq T \leq 500$ K. The results are shown in Fig. 5. At 300 K, ZCT gives the tunneling correction as 11.3, underestimating the tunneling effect by a factor of 2.6 as compared with the SCT method. Meanwhile, the Eckart model performs much better than ZCT. Fig. 5 implies that any future theoretical studies of the H-migration reactions of peroxy radicals from isoprene need to pay more attention to the treatment of tunneling.

3.3 Hindered rotor effect

To calculate hindered rotor partition functions for use in eqn (10), hindrance potentials for the –CH_3, –OO and –CH_2CH_3 rotors of the 1-propylperoxy radical were

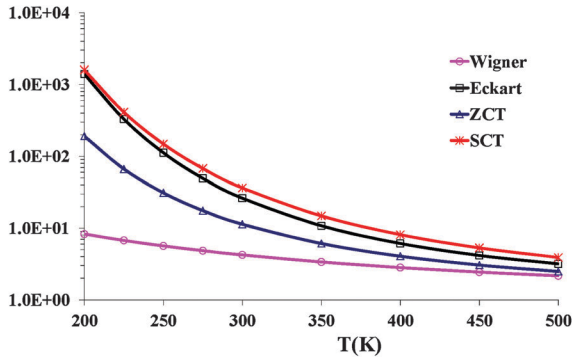

Fig. 5 Tunneling coefficient of 1,5 H-migration with different approximations in the temperature range 200–500 K.

investigated by 10° resolution relaxed scans at M052X, B3LYP, and B1B95 with the MG3S basis set. For the saddle points for 1,4 H-migration and HO_2 elimination, the rotation of –CH_3 was scanned at B3LYP/MG3S and B1B95/MG3S, respectively. No hindered rotor was identified for the saddle point for 1,5 H-migration due to its six membered ring structure. Fig. 6 illustrates the optimized geometry, internal

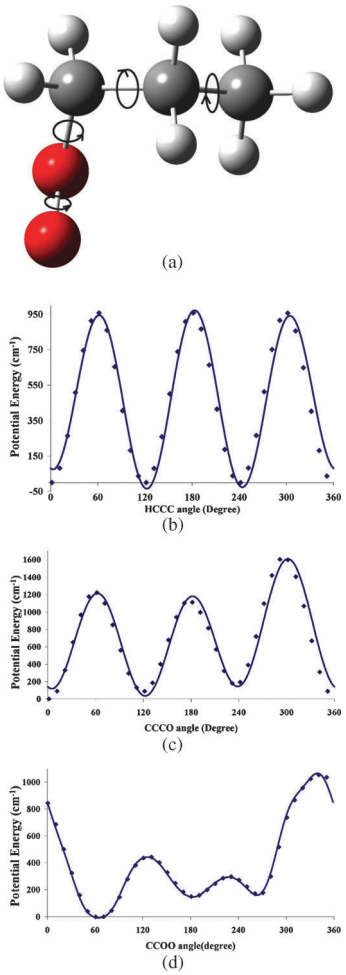

Fig. 6 (a) Optimized geometry of the 1-propylperoxy radical, showing torsions (b)–(d) hindrance potentials of CCCH, CCCO, and CCOO rotation at M05-2X/MG3S. The 10° resolution scanning data are shown in dots, fitted Fourier series are shown in solid line.

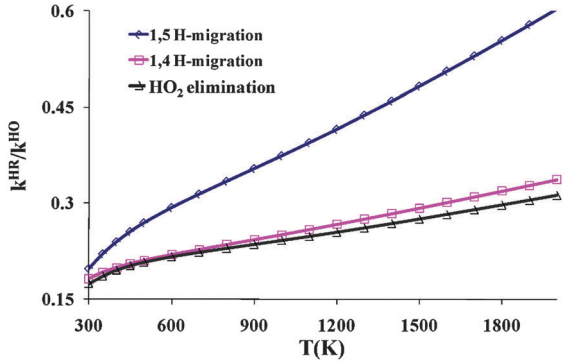

Fig. 7 Ratio of rate constants by HR and HO treatments for the three reactions

rotations, and rotational potentials for the lowest energy conformer of the reactant. The Fourier series fit of the potential matches very well with the scanning data. Treating the coupling of the $-CH_2CH_3$ and –OO torsions would require a multidimensional hindered-rotor treatment, which is beyond the scope of the present work.[22]

Fig. 7 illustrates the temperature dependence of the ratio of k^{HR} to k^{HO}, *i.e.* $C(T)$ in eqn (10). The reactant always has more internal rotors than the saddle point, so $C(T)$ does not exceed unity. The hindered rotor effect is most important at low temperatures. The inclusion of the hindered rotor correction *via* eqn (10) decreases the computed rate constant at 2000 K by a factor of 1.7 for the 1,5 H-migration, 3.0 for the 1,4 H-migration and 3.2 for the HO_2 elimination; the decreases are factors of 5.0–5.7 at 300 K. At high temperature $C(T)$ for 1,5 H-migration is closer to unity than the other two reactions, which can be explained by the absence of internal rotation in the transition state for 1,5 H-migration.

3.4 High-pressure limiting rate constants

High-pressure limiting (HPL) rate constants for R1 to R3 were computed by CVT/SCT with hindered rotor corrections in the temperature range of 500–2000 K. The results are shown in Fig. 8, along with the results of two other recent studies.[8,14] Clearly, the 1,5 H-migration channel dominates the reactivity below 1000 K because of its low barrier height. However, the rate constant of the HO_2 elimination tends to exceed that of the 1,5 H-migration above 1200 K, because the pre-exponential factor for HO_2 elimination is much larger than that for 1,5 H-migration. A significant contribution to the low

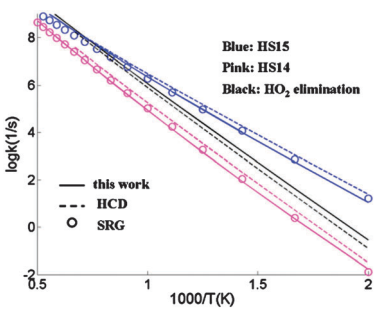

Fig. 8 Comparison of computed HPL rate constants between this work and previous theoretical studies (ref. 8 and 14).

Table 3 The fitted parameters using two modified Arrhenius equations for R1–R3 within 500–2000 K (A is in s^{-1}, E in kcal mol^{-1}; T_0 in K)

	R1	R2	R3
Model 1 $k = A(\frac{T}{300})^n e^{-\frac{E}{RT}}$			
A	5.200×10^9	2.020×10^9	4.079×10^{11}
n	2.361	2.888	1.303
E	21.011	26.870	28.431
RMSR[a]	0.012	0.041	0.008
Model 2 $k = A(\frac{T}{300})^n e^{-\frac{E(T+T_0)}{R(T^2+T_0^2)}}$			
A	5.261×10^8	5.038×10^8	1.102×10^{10}
n	3.049	3.088	2.460
E	15.835	21.189	21.233
T_0	178.94	220.58	159.50
RMSR	0.008	0.009	0.008

[a] RMSR = root mean square residual.

pre-exponential factor of 1,5 H-migration is the absence of a hindered rotor in its transition state. As a side note, variational effects on the rate constant for the two H-migration reactions are very small in the whole temperature range studied (<1%). The variational treatment makes a larger difference for HO_2 elimination due to its relatively loose transition state structure, but the effect is still less than 3% at the highest temperature considered here. Table 3 lists the fitted parameters of two modified Arrhenius equations for the same temperature range. Model 2, with one more parameter than Model 1, was recently proposed by Zheng and Truhlar[27] to give small error and correct low-temperature behaviour for the activation energy and rate constant.

Recently, two other groups[8,14] computed HPL rate constants for the unimolecular reactions of the 1-propylperoxy radical by conventional transition state theory using the CBS-QB3 method. CBS-QB3 performs well as compared to our benchmark CCSD(T) calculation (see ESI† for details). Fig. 6 illustrates the comparison between this work, that of Huynh, Carstensen and Dean (HCD)[8] and Sharma, Raman, and Green (SRG).[14] These three works all used the TES hindered rotor treatment. SRG used Wigner's approximation for tunneling effects but HCD used the asymmetric Eckart potential. Taking into account the differences in methodology, the three theoretical studies give quite satisfactory results with the largest deviation less than a factor of 2 over the temperature range studied.

4. Conclusions

This work presents computations of the extent of temperature-dependent tunneling for HO_2 elimination and 1,4 and 1,5 H-migration reactions of the 1-propylperoxy radical using small curvature tunneling. The DFT methods and basis sets are chosen for reasonable agreement with barrier heights and reaction energies of the same three reactions computed by a high level benchmark. For the reactions studied, the tunneling corrections, $\kappa(T)$, determined from the asymmetric Eckart approach provide good estimates of the SCT results, while ZCT and Wigner grossly underestimate tunneling effects. As discussed in the text, this conclusion does not hold generally, and the reliability of Eckart tunneling coefficients, $\Gamma(E)$, is not

nearly so good. The variation in the sign and extent of error in Eckart tunneling coefficients, $\Gamma(E)$, casts some doubt on the reasonableness of assuming that $\kappa(T)$ from the Eckart method is reliable for H-migration reactions of other peroxy radicals besides 1-propylperoxy.

HPL rate constants for these three reactions were obtained by CVT/SCT, and our results agree well with previous theoretical studies. Tunneling effects are expected to be even more important in the fall-off region than in the high-pressure limit, and rate constants for peroxy radical reactions relevant to diesel ignition are commonly in the fall-off region under realistic conditions. Hindered rotor effects, as expected, significantly affect rate constants.

Acknowledgements

We appreciate Prof. Donald G. Truhlar and Dr Jing-Jing Zheng for providing us the POLYRATE program and many useful suggestions. Prof. William H. Green shared his thoughts on hindered rotor treatments with us, and two anonymous referees helped improve this manuscript. This work was supported by the US Department of Energy under grant DE-SC0002511 and the National Science Foundation through TeraGrid resources provided by the NCSA under grant number TG-CHE080012P.

References

1 *Low-Temperature Combustion and Autoignition*, ed. M. J. Pilling, Elsevier, Amsterdam, 1997, p. XIII.
2 C. J. Hayes, J. K. Merle and C. M. Hadad, *Adv. Phys. Org. Chem.*, 2008, **43**, 79.
3 D. R. Glowacki and M. J. Pilling, *ChemPhysChem*, 2010, **11**, 3836.
4 F. Buda, R. Bounaceur, V. Warth, P. A. Glaude, R. Fournet and F. Battin-Leclerc, *Combust. Flame*, 2005, **142**, 170.
5 F. Battin-Leclerc, O. Herbinet, P. Glaude, R. Fournet, Z. Zhou, L. Deng, H. Guo, M. Xie and F. Qi, *Angew. Chem., Int. Ed.*, 2010, **49**, 3169.
6 C. A. Taatjes, *J. Phys. Chem. A*, 2006, **110**, 4299.
7 E. G. Estupiñán, S. J. Klippenstein and C. A. Taatjes, *J. Phys. Chem. A*, 2005, **109**, 8374.
8 L. K. Huynh, H. Carstensen and A. M. Dean, *J. Phys. Chem. A*, 2010, **114**, 6594.
9 S. J. Klippenstein, L. B. Harding, M. J. Davis, A. S. Tomlin and R. T. Skodje, *Proc. Combust. Inst.*, 2011, **33**, 351.
10 R. T. Skodje, A. S. Tomlin, S. J. Klippenstein, L. B. Harding and M. J. Davis, *J. Phys. Chem. A*, 2010, **114**, 8286.
11 H. Machrafi and S. Cavadias, *Combust. Flame*, 2008, **155**, 557.
12 M. Yao, Z. Zheng and H. Liu, *Prog. Energy Combust. Sci.*, 2009, **35**, 398.
13 A. C. Davis and J. S. Francisco, *J. Phys. Chem. A*, 2010, **114**, 11492.
14 S. Sharma, S. Raman and W. H. Green, *J. Phys. Chem. A*, 2010, **114**, 5689.
15 F. Zhang and T. S. Dibble, *J. Phys. Chem. A*, 2011, **115**, 655.
16 H. Carstensen, C. V. Naik and A. M. Dean, *J. Phys. Chem. A*, 2005, **109**, 2264.
17 L. Zhu, J. W. Bozzelli and L. M. Kardos, *J. Phys. Chem. A*, 2007, **111**, 6361.
18 S. V. Petway, H. Ismail, W. H. Green, E. G. Estupiñán, L. E. Jusinski and C. A. Taatjes, *J. Phys. Chem. A*, 2007, **111**, 3891.
19 A. Miyoshi, *Int. J. Chem. Kinet.*, 2010, **42**, 273.
20 E. Wigner, *Z. Phys. Chem., Abt. B*, 1932, **19**, 203.
21 C. Eckart, *Phys. Rev.*, 1930, **35**, 1303.
22 A. Fernández-Ramos, B. A. Ellingson, B. C. Garret and D. G. Truhlar, in *Reviews in Computational Chemistry*, ed. T. R. Cundari and K. B. Lipkowitz, Wiley-VCH, Hoboken, NJ, 2007, vol. 23, p. 125.
23 R. T. Skodje and D. G. Truhlar, *J. Phys. Chem.*, 1981, **85**, 624.
24 B. C. Garret and D. G. Truhlar, in *Theory and Applications of Computational Chemistry: The first Forty Years*, ed. C. Dykstra, G. Frenking, K. S. Kim and G. E. Scuseria, Elsevier B. V., 2005, p. 67.
25 D. G. Truhlar and A. Kuppermann, *J. Am. Chem. Soc.*, 1971, **93**, 1840.
26 R. Meana-Pañeda, D. G. Truhlar and A. Fernández-Ramos, *J. Chem. Theory Comput.*, 2010, **6**, 6.
27 J. Zheng and D. G. Truhlar, *Phys. Chem. Chem. Phys.*, 2010, **12**, 7782.
28 V. D. Knyazev and I. R. Slagle, *J. Phys. Chem.*, 1996, **100**, 16899.
29 P. Zhang and C. K. Law, *Int. J. Chem. Kinet.*, 2011, **43**, 31.
30 J. D. DeSain, C. A. Taatjes, J. A. Miller, S. J. Klippensteina and D. K. Hahn, *Faraday Discuss.*, 2001, **119**, 101.
31 J. D. DeSain, E. P. Clifford and C. A. Taatjes, *J. Phys. Chem. A*, 2001, **105**, 3205.
32 J. D. DeSain, S. J. Klippenstein, J. A. Miller and C. A. Taatjes, *J. Phys. Chem. A*, 2003, **107**, 4415.
33 H. Huang, D. J. Merthe, J. Zádor, L. E. Jusinski and C. A. Taatjes, *Proc. Combust. Inst.*, 2011, **33**, 293.
34 M. J. Frisch, G. W. Trucks, H. B. Schlegel, G. E. Scuseria, M. A. Robb, J. R. Cheeseman, G. Scalmani, V. Barone, B. Mennucci, G. A. Petersson, H. Nakatsuji, M. Caricato, X. Li, H. P. Hratchian, A. F. Izmaylov, J. Bloino, G. Zheng, J. L. Sonnenberg, M. Hada, M. Ehara, K. Toyota, R. Fukuda, J. Hasegawa, M. Ishida, T. Nakajima, Y. Honda, O. Kitao, H. Nakai, T. Vreven, J. A. Montgomery, Jr., J. E. Peralta, F. Ogliaro, M. Bearpark, J. J. Heyd, E. Brothers, K. N. Kudin, V. N. Staroverov, R. Kobayashi, J. Normand, K. Raghavachari, A. Rendell, J. C. Burant, S. S. Iyengar, J. Tomasi, M. Cossi, N. Rega, J. M. Millam, M. Klene, J. E. Knox, J. B. Cross, V. Bakken, C. Adamo, J. Jaramillo, R. Gomperts, R. E. Stratmann, O. Yazyev, A. J. Austin, R. Cammi, C. Pomelli, J. W. Ochterski, R. L. Martin, K. Morokuma, V. G. Zakrzewski, G. A. Voth, P. Salvador, J. J. Dannenberg, S. Dapprich, A. D. Daniels, Ö. Farkas, J. B. Foresman, J. V. Ortiz, J. Cioslowski and D. J. Fox, *Gaussian 09, Revision A.1*, Gaussian Inc., Wallingford, CT, 2009.
35 L. Simón and J. M. Goodman, *Org. Biomol. Chem.*, 2011, **9**, 689.
36 Y. Zhao, N. E. Schultz and D. G. Truhlar, *J. Chem. Phys.*, 2005, **123**, 161103.
37 Y. Zhao, N. E. Schultz and D. G. Truhlar, *J. Chem. Theory Comput.*, 2006, **2**, 364.
38 K. Raghavachari, G. W. Trucks, J. A. Pople and M. Head-Gordon, *Chem. Phys. Lett.*, 1989, **157**, 479.
39 E. Papajak, H. R. Leverentz, J. Zheng and D. G. Truhlar, *J. Chem. Theory Comput.*, 2009, **5**, 1197.
40 Y. Zhao and D. G. Truhlar, *Theor. Chem. Acc.*, 2008, **120**, 215.
41 A. D. Becke, *J. Chem. Phys.*, 1993, **98**, 5648.
42 C. T. Lee, W. T. Yang and R. G. Parr, *Phys. Rev. B*, 1988, **37**, 785.
43 A. D. Boese and J. M. L. Martin, *J. Chem. Phys.*, 2004, **121**, 3405.
44 J. P. Perdew and Y. Wang, *Phys. Rev. B: Condens. Matter*, 1992, **45**, 13244.
45 J. Perdew, K. Burke and M. Ernzerhof, *Phys. Rev. Lett.*, 1997, **78**, 1396.
46 J. D. Chai and M. Head-Gordon, *J. Chem. Phys.*, 2008, **128**, 084106.
47 A. D. Becke, *J. Chem. Phys.*, 1996, **104**, 1040.
48 H. L. Schmider and A. D. Becke, *J. Chem. Phys.*, 1998, **108**, 9624.
49 T. Yanai, D. Tew and N. Handy, *Chem. Phys. Lett.*, 2004, **393**, 51.
50 A. Fernández-Ramos, B. A. Ellingson, R. Meana-Pañeda, J. M. C. Marques and D. G. Truhlar, *Theor. Chem. Acc.*, 2007, **118**, 813.
51 J. Zheng, S. Zhang, B. J. Lynch, J. C. Corchado, Y.-Y. Chuang, P. L. Fast, W.-P. Hu, Y.-P. Liu, G. C. Lynch, K. A. Nguyen, C. F. Jackels, A. F. Ramos, B. A. Ellingson, V. S. Melissas, J. Villa, I. Rossi, E. L. Coitino, J. Pu, T. V. Albu, R. Steckler, B. C. Garrett, A. D. Isaacson and D. G. Truhlar, *POLYRATE-version 2009-A*, University of Minnesota, Minneapolis, 2010.
52 J. Zheng, S. Zhang, J. C. Corchado, Y. Chuang, E. L. Coitiño, B. A. Ellingson and D. G. Truhlar, *GAUSSRATE-version 2009-A*, University of Minnesota, Minneapolis, 2010.
53 M. Page and J. W. McIver, Jr., *J. Chem. Phys.*, 1988, **88**, 922.
54 J. C. Corchado, E. L. Coitiño, Y.-Y. Chuang, P. L. Fast and D. G. Truhlar, *J. Phys. Chem. A*, 1998, **102**, 2424.

55 Y.-Y. Chuang and D. G. Truhlar, *J. Phys. Chem. A*, 1998, **102**, 242.
56 I. M. Alecu, J. Zheng, Y. Zhao and D. G. Truhlar, *J. Chem. Theory Comput*., 2010, **6**, 2872The data base is available at http://comp.chem.umn.edu/freqscale/index.html.
57 B. C. Garrett and D. G. Truhlar, *J. Phys. Chem*., 1979, **83**, 2921.
58 A. G. Vandeputte, M. K. Sabbe, M.-F. Reyniers, V. V. Speybroeck, M. Waroquier and G. B. Marin, *J. Phys. Chem. A*, 2007, **111**, 11771.
59 D. G. Truhlar, *et al*., *J. Chem. Soc., Faraday Trans*., 1994, **90**, 1733.
60 A. Fernández-Ramos, *J. Chem. Theory Comput*., 2005, **1**, 1063.
61 Y.-P. Liu, D. H. Lu, A. González-Lafont, D. G. Truhlar and B. C. Garrett, *J. Am. Chem. Soc*., 1993, **115**, 7806.
62 A. Miyoshi, UNIMOL package is availabe at http://www.frad.t.u-tokyo.ac.jp/~miyoshi/ssumes/.
63 K. S. Pitzer and W. D. Gwinn, *J. Chem. Phys*., 1942, **10**, 428.
64 C. Y. Lin, E. I. Izgorodina and M. L. Coote, *J. Phys. Chem. A*, 2008, **112**, 1956.
65 T-Chem is the program to calculate thermochemistry data for harmonic oscillator, hindered rotor, and free rotor corrections. It's avalible at http://rsc.anu.edu.au/~cylin/scripts.php.
66 S. H. Mousavipour, A. Fernández-Ramos, R. Meana-Pañeda, E. Martínez-Núñez, S. A. Vázquez and M. A. Ríos, *J. Phys. Chem. A*, 2007, **111**, 719.
67 J. Pfaendtner and L. J. Broadbelt, *Chem. Eng. Sci*., 2007, **62**, 5232.
68 R. Méreau, M.-T. Rayez, F. Caralp and J.-C. Rayez, *Phys. Chem. Chem. Phys*., 2003, **5**, 4828.
69 R. Meana-Pañeda, D. G. Truhlar and A. Fernández-Ramos, *J. Chem. Phys*., 2011, **134**, 094302.
70 J. Peeters, T. L. Nguyen and L. Vereecken, *Phys. Chem. Chem. Phys*., 2009, **11**, 5935.
71 J. Peeters and J.-F. Müller, *Phys. Chem. Chem. Phys*., 2010, **12**, 14227.
72 A. Guenther, T. Karl, P. Harley, C. Wiedinmyer, P. I. Palmer and C. Geron, *Atmos. Chem. Phys*., 2006, **6**, 3181.
73 J. Lelieveld, T. M. Butler, J. N. Crowley, T. J. Dillon, H. Fischer, L. Ganzeveld, H. Harder, M. G. Lawrence, M. Martinez, D. Taborelli and J. William, *Nature*, 2008, **252**, 737.
74 T. L. Nguyen, L. Vereecken and J. Peeters, *ChemPhysChem*, 2009, **12**, 7782.